Latin American Journal of Solids and Structures
www.lajss.org

A numerical study on the impact behavior of foam-cored cylindrical sandwich shells subjected to normal/oblique impact

Abstract

Finite element analysis was used to investigate the impact behavior of the foam-cored sandwich shells under the ballistic impact. The ballistic limit, failure mode of the face-sheet and energy absorption of the uniform/graded core were discussed in this paper. Based on the impact phase diagrams, the effects of several factors (i.e. projectile shape and diameter, face-sheet curvature and thickness) on the normal/oblique impact behavior were analyzed in detail. Results indicate that blunter and larger projectiles, higher impact velocity and thicker face-sheets can significantly raise the impact-resistance performance of the targets. In addition, the behavior of ballistic impact becomes more complex as the result of the increasing oblique angle.

Keywords

Cylindrical sandwich shells; aluminium foam; oblique impact; impact phase diagram; numerical simulation.

Buyun Su[a]
Zhiwei Zhou[b]
Jianjun Zhang[c]
Zhihua Wang[d]
Xuefeng Shu[e*]
Zhiqiang Li[f]

[a,c,d,e,f]Institute of Applied Mechanics and Biomedical Engineering, Taiyuan University of Technology, Taiyuan 030024, China
[b]State Key Laboratory of Frozen Soil Engineering, Cold and Arid Regions Environmental and Engineering Research Institute, Chinese Academy of Sciences, Lanzhou 730000, China

Corresponding author:
[e*]shuxuefeng@tyut.edu.cn

http://dx.doi.org/10.1590/1679-78251742

Received 01.12.2014
In revised form 23.05.2015
Accepted 29.05.2015
Available online 07.07.2015

1 INTRODUCTION

Sandwich structures are widely used in various engineering applications such as protective structures of autos and aircrafts, due to their excellent energy absorption capability, high specific strength and superior shock-resistance characteristics under such extreme loading as blast or ballistic impact (Ashby et al., 2000; Lu and Yu, 2003; Gibson and Ashby, 1997). Sandwich structures usually consist of two face-sheets with identical thickness and a cellular core. The face-sheets are usually made of metal, ceramic, fibre-reinforced composite or laminate, and the cores are commonly made of foams,

honeycombs or polymer (Deshpande and Fleck, 2000; Zhou et al., 2012a; 2012b; Shen et al., 2010a). The performance of sandwich structures with an aluminium foam core and aluminium alloy sheets under low and high-velocity impact loading were analyzed by various experiments and numerical simulations. Various works of literature focused on the typical deformation/failure modes, failure mechanism and energy absorption of the sandwich structures (Cho et al., 2012; Dean et al., 2011; Qiu and Fleck, 2003; Shen et al., 2010b; Shen et al., 2015; Li et al., 2014). In particular, an analytical model developed by Fleck and Deshpande (2004) has become a theoretical frame for studying the dynamic response of sandwich structures. Hanssen et al. (2006) simulated the bird strike on sandwich panels with aluminium foam core and sheets and compared the results with the experimental measurements. Mohan et al. (2011) analyzed the impact response of foam with different face sheets and compared the initiating failure mechanisms of them. Buitrago et al. (2010) and Ivañez et al. (2011) investigated the dynamic response and energy absorption of composite sandwich panels with honeycomb/foam core under high-velocity impact. The simulation results indicated that the damaged regions of the skins and the core were concentrated in a small area around the impact point and that most of the impact energy was absorbed by the face-sheets; as a result, the influence of the foam core is negligible. Moreover, much research has proven that the effects of the strain rate, inertia and stress wave have gradually become considerable with the increase in impact velocity. Meanwhile, Zhao et al. (2007) set up an experiment to investigate the perforation of aluminium foam core sandwich panels using a split Hopkinson pressure bar and predicted the dynamic perforation energy of the sandwich structure that is larger than its quasi-static dissipation because of the inertia effect. Tan et al. (2005) developed an R-P-P-L model to investigate the elastic–plastic stress wave propagation into a uniform foam. According to the mechanism of the R-P-P-L model and plastic structural shock theory, Lu et al. (2008) accurately predict the resistance force with depth during the indentation process.

The properties of sandwich structures under the projectile impact are strongly influenced by many parameters, such as the relative density of the foam cores, the thickness of the face-sheet, the dimensions of the sandwich structures and the geometry of the projectiles (Gupta et al., 2008; Senthil and Iqbal, 2013). These parameters must be taken into consideration during engineering design and application. Hou et al. (2010) carried out ballistic impact experiments of sandwich panels with aluminium foam core, and discussed the effects of different key parameters on the ballistic performance and energy absorption of the sandwich panels systematically. However, it should be noted that the existing work mainly focused on the sandwich panels, and much was limited in terms of the properties of the sandwich shells under the blast loading/normal impact (Jing et al., 2011; Mozafari et al., 2015). Actually, the sandwich shells have greater far-ranging applications than sandwich beams/panels and many practical engineering applications are more easily subjected to oblique impact (Iqbal et al., 2010). On the other hand, related literature in this field is greatly limited.

The main aim of the present paper is to investigate the impact behavior of cylindrical sandwich shell structures under the ballistic impact with different oblique angles. Section 2 is where the geometry model and material properties are presented. In order to validate the numerical models, the numerical results are compared with the experimental tests in Section 3. Furthermore, in Section 4, the ballistic limit, residual velocity and energy absorption of the uniform/graded core are discussed. Moreover, the impact-resistance performance of the targets are analyzed by using the impact phase diagrams. Details are given in the following sections.

2 GEOMETRY MODEL AND MATERIAL PROPERTIES

2.1 Modeling geometry

The numerical model was established by using the non-linear, explicit FE code LS-DYNA (Version ls-971). Projectiles were adopted as rigid bodies and the target was used as a deformable body in this simulation model. Since the sandwich shell structure and projectile are geometrical symmetry, only half of the structure was employed, as shown in Figure 1(a). The sandwich shell structure is composed of two aluminium face-sheets with identical thickness and an aluminium foam core. Meanwhile, the dimensions of the sandwich shell were 100×100 mm, according to the experimental structure parameters obtained from the literature (Hou et al., 2010), and the foam core, which held a relative density of 20%, was built with 30 mm of thickness.

In order to investigate the effects of the geometrical sandwich shell's parameters in detail, the face-sheets were established with three thicknesses H (0.8 mm, 1 mm, 1.2 mm) and three curvatures K (8/m, 4/m, 0/m). Here, $K = 8/\mathrm{m}$ and $K = 4/\mathrm{m}$ indicate that the radius of the curvature of the middle surface of the core is 125 mm and 250 mm, respectively. $K = 0/\mathrm{m}$ denotes the sandwich panel. Meanwhile, the effects of the gradient foam core were considered in the simulation. The graded foam core consists of three core layers with a relative density of 10%, 15% and 20%, respectively; the thickness of each core layer was 10 mm, as shown in Figure 1(b).

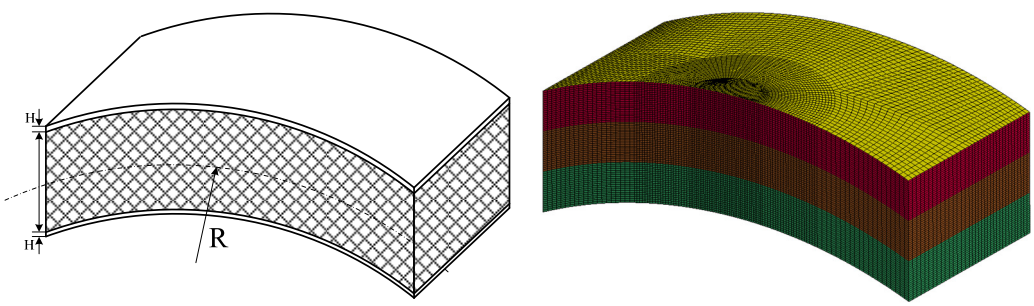

(a) (b)

Figure 1: (a) Sketch of the 1/2 sandwich shell structure.
(b) FE model of the 1/2 sandwich shell structure with graded foam core.

In addition, the influence of projectiles on the ballistic impact cannot be ignored. Therefore, the steel projectiles were established with three shapes (i.e, flat nosed, hemispherical nosed and conical nosed) in the present study. Furthermore, hemispherical nosed projectiles were established with three diameters D (8 mm, 9 mm, 10 mm). In order to ensure the whole system with the same initial kinetic energy, all of the projectiles were established with identical mass. The geometries and dimensions of each kind of the projectiles ($D =$ 8 mm) are shown in Figure 2, respectively.

The sandwich shell face-sheets were modeled by the Belytschko-Tasy shell element and the foam core was modeled by the default brick element. The number of shell elements and the amount of solid elements were 8,256 and 247,680, respectively. Mesh sensitivity studies indicated that further refinement does not significantly improve the accuracy of the calculations. The meshed model is shown in Figure 1(b).

2.2 Material properties

The aluminum foam core was represented by material model 63 of LS_DYNA (MAT_CRUSHALBE_FOAM), which is dedicated to modeling crushable foam with optional damping and tension cutoff. In this model, tension is treated as elastic-perfectly-plastic at the tension cut-off value (manual, 2012). The material parameters of foam cores were obtained by standard quasi-static tests. The quasi-static uniaxial compressive stress-strain curves of the foam with three different relative densities (10%, 15%, and 20%) are plotted in Figure 3. Here, maximum shear strain (MSS=0.4) was used to define the failure criteria of the foam core (Jing et al., 2013).

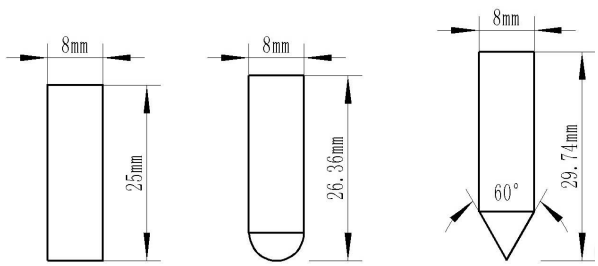

Figure 2: Dimensions of the three kinds of projectiles: flat nosed; hemispherical nosed and conical nosed.

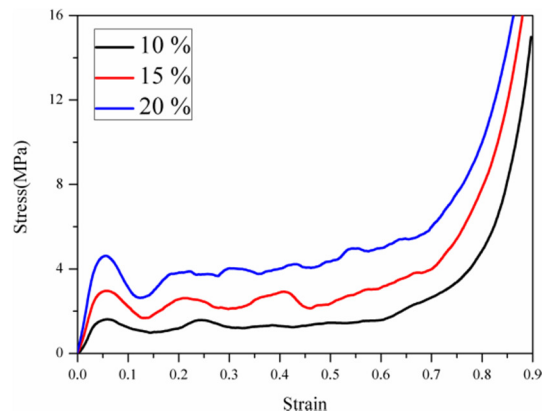

Figure 3: Quasi-static compressive stress-strain curves of aluminum foam cores used in the simulation.

The aluminium alloy face-sheets were represented by material model 104 of LS_DYNA (MAT_DAMAGE_1). This model is based on the continuum damage theory (manual, 2012). The effective stress $\tilde{\sigma}$ is defined as

$$\tilde{\sigma} = \frac{\sigma}{1-D} = Y^0 + Q_1\left[1-\exp\left(-c_1 r\right)\right] + Q_2\left[1-\exp\left(-c_2 r\right)\right] \tag{1}$$

where D is the isotropic damage variable, σ is the true stress, and r is the damage accumulated in the plastic strain. Here, the rate of the damage-accumulated strain is given by $\dot{r} = \left(1-D\right)\dot{\varepsilon}_{pl}$, and $\dot{\varepsilon}_{pl}$ is the usual measure for the rate of the accumulated plastic strain. An evolution rule of the damage variable D is expressed by

$$D = \begin{cases} 0 & \text{for } r \le r_D \\ \dfrac{Y}{S(1-D)}\dot{r} & \text{for } r > r_D \end{cases} \tag{2}$$

where r_D is the damage threshold, S is a positive material constant and the strain energy density release rate of Y is

$$Y = \frac{\sigma_{vm}^2 R_v}{2E\left(1-D\right)^2} \text{ , and } R_v = \frac{2}{3}\left(1+v\right) + 3\left(1-2v\right)\left(\frac{p}{\sigma_e}\right)^2 \tag{3}$$

where σ_{vm} is the equivalent von Mises stress, R_v is the triaxiality function, and v is the Poisson's ratio. The failure criteria is given by $D = D_C$, where D_C is a material constant denoted as the critical damage.

The material parameters of the above equations were used: $\rho = 2700$ kg/m^3, $E = 70$ GPa, $v = 0.3$, $Y^0 = 70$ MPa, $Q_1 = 334.7$ MPa, $c_1 = 6.16$, $Q_2 = 0$ MPa, $c_2 = 0$, $r_D = 0.18$, $S = 0.5$ MPa, and $D_C = 0.1$. Here, it should be pointed out that the strain-rate effects of the materials have been neglected.

3 VALIDATION OF NUMERICAL METHOD

3.1 Validation of failure mode

Ballistic impact experiments of metallic sandwich panels with aluminium foam core were studied by Hou et al. (2010). According to the dimensions and parameters of sandwich panels obtained from literature (Hou et al., 2010), the FE model was established to validate the present numerical approach. The typical failure mode of the target in the experiment was compared with the FE prediction result, as shown in Figure 4. It can be clearly seen that the front sheet presents a circular crater, a localised tunnel can be observed in the foam core and the back sheet failed with petal formation. The figure shows that the numerically predicted failure modes agree well with the experimental data.

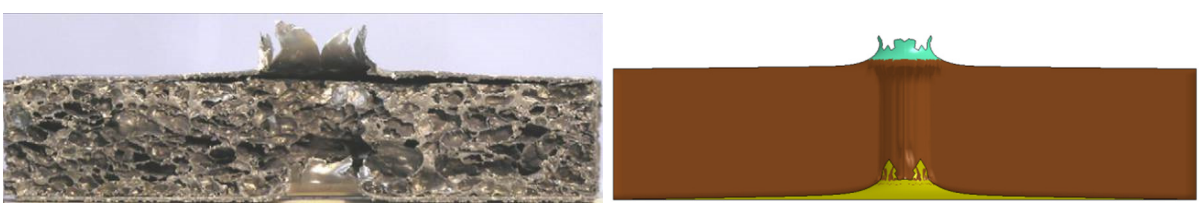

Figure 4: Experimental and numerical failure mode of sandwich panels.

3.2 Validation of the dynamic enhancement factor

The energy absorbed by the structure during perforation is called the perforation energy. Since the mass of any small fragmentations during perforation is neglected, the perforation energy can be calculated by the Eq. (4.a).

$$\frac{1}{2}m_p V_i^2 - \frac{1}{2}m_p V_r^2 = E_p \tag{4.a}$$

$$\Phi = \frac{E_d}{E_s} \tag{4.b}$$

Here, m_p is the mass of the projectile, E_p is the perforation energy, and V_i and V_r are the impact velocity and residual velocity, respectively. The ratio of dynamic and quasi-static perforation energy (E_d/E_s) is defined as a dynamic enhancement factor Φ. Φ is a dimensionless parameter, and reflects the relationship between impact velocity and energy absorption of the sandwich structure, namely the inertia effect of the structure. Additionally, the enhancement factors obtained by the numerical prediction and the experimental measurements were summarized in Figure 5. The results illustrate that the parameter Φ notably increases with the increasing impact velocity. In other words, higher impact velocity can significantly raise the energy absorption of the sandwich structure. This conclusion is in good agreement with the experimental results (Zhao et al., 2007; Hou et al., 2010).

4 RESULTS AND DISCUSSION

In this paper, the initial velocity direction and the axis of the projectile are coincident. The oblique angle θ is defined as the acute angle between the velocity vector of the projectile and the outward normal vector of the target, as shown in Figure 6. An oblique angle equaling to zero means the normal impact. The effects of the projectile nose shape and the graded foam core on the impact-resistance performance of the sandwich shells are presented detailly in Sections 4.1 and 4.2, respectively; certain key parameters are kept constant as $K = 4/\text{m}$, $H = 1$ mm and $D = 8$ mm. Then, in Section 4.3, the impact phase diagram is introduced to further analyze the cases of oblique impact; and the effects of a series of parameters on impact behavior were studied in detail.

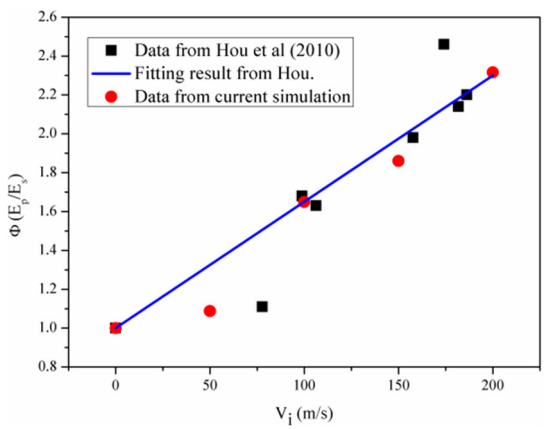

Figure 5: Comparison of experimental and predicted enhancement factors of sandwich panels.

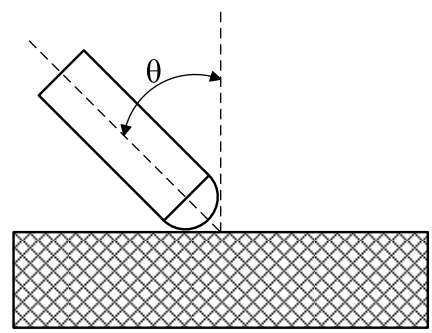

Figure 6: Sketch of the penetration angle of the projectile.

4.1 Effects of the projectile nose shapes on the normal impact behavior

4.1.1 Ballistic limit and residual velocity

The present simulation results in terms of residual velocities under normal impact are illustrated in Figure 7. It is clearly observed from Figure 7 that the ballistic limit of the flat nosed projectile is the highest. Compared with flat nosed projectile, the ballistic limits of the hemispherical and conical nosed projectile are reduced by 40% and 50%, respectively. And the residual velocities of the three different projectiles become gradually closer to each other with the increase in impact velocity. The

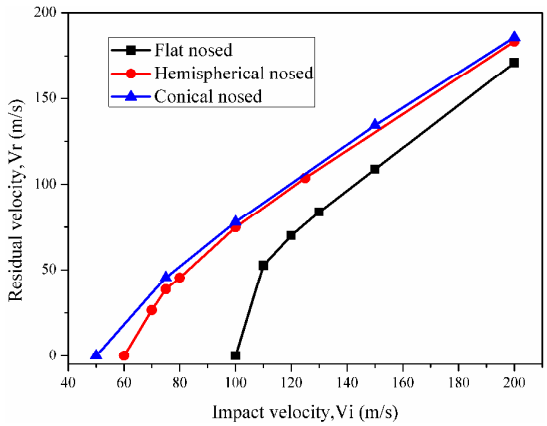

Figure 7: Comparison of residual velocity with different projectiles.

residual velocities of the hemispherical and conical nosed projectiles in particular are approximately equal when the impact velocity exceeds 80 m/s. This means the effect of the projectile shape can be ignored if the impact velocity is sufficiently high.

The above phenomena clearly reveals that the blunter projectiles can effectively increase the ballistic limit and lower the residual velocity when the impact velocity is constant. This conclusion is in agreement with the experimental results (Zhao et al., 2007; Hou et al., 2010).

4.1.2 Failure mode of the face-sheet

The deformation processes of sandwich shells under different nosed projectiles impact are shown in Figure 8. The projectiles always follow a central axis while penetrating their target under normal impact. All of the front face-sheets show a circular crater and a localised tunnel is exhibited in the foam cores. In addition, the failure modes of the back face-sheet are strongly affected by the projectile nose shapes. For the case of impact by flat nosed projectiles, a circular cap of diameter equal to that of the projectile was removed from the face-sheet. Additionally, the hemispherical nosed projectile failed the face-sheet by the formation of petals. For the conical nosed projectile, a small hole was produced at the initial stage of the impact; then, the hole progressively enlarged until its diameter was equal to that of the projectile. The above failure modes are called plugging, petaling and hole enlargement, respectively. The bottom row of Figure 8 shows that the plastic deformation area caused by the flat nosed projectile is the largest, followed by the hemispherical nosed and then the conical nosed. This means that blunter projectiles could result in larger deformation areas, further leading to a larger ballistic limit and higher energy absorption ability. Moreover, the interfacial failure can be observed between the back face-sheet and the core is essentially a result of tensile failure of the foam core caused by the deformation of the back face-sheet.

4.2 Effects of the graded foam core on the normal impact behavior

Here, a qualitative study was carried out to analyze the energy absorption of sandwich shells with the uniform and graded core (Figure 1) during the normal impact process (the impact velocity is 100 m/s). The relative density of the uniform core was 15% (Group 1) and six groups of graded

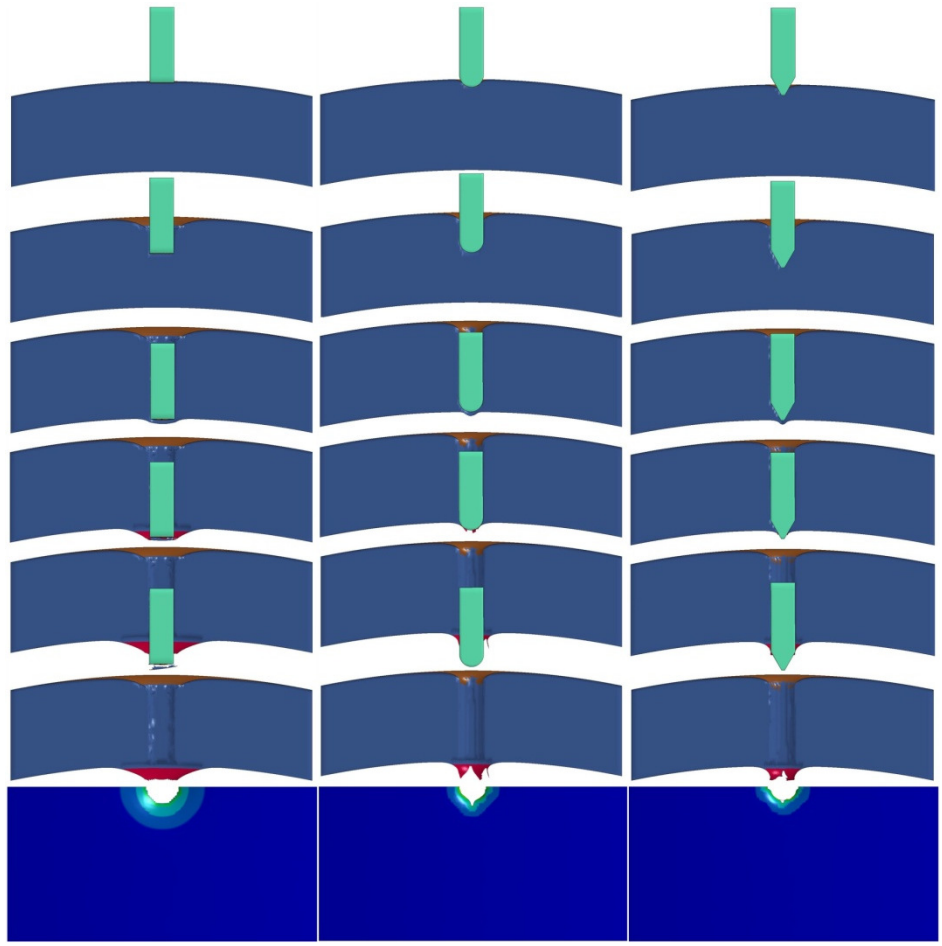

Figure 8: The deformation process of sandwich shells under normal impact by different projectiles: (a) flat nosed; (b) hemispherical nosed; (c) conical nosed, and the effective plastic strain of back face-sheet (bottom row).

Groups	1	2	3	4	5	6	7
Front layer	15%	10%	10%	15%	15%	20%	20%
Middle layer	15%	15%	20%	10%	20%	10%	15%
Back layer	15%	20%	15%	20%	10%	15%	10%

Table 1: Relative density of the graded foam core for sandwich shell structure.

foam cores (Groups 2 to 7) were employed by arranging the three core layers with different relative densities (Table 1). It should be noted that three relative densities (10%, 15% and 20%) for graded foam cores were selected to ensure that all the structures had the same mass.

The typical evolution of the energy of the entire system during the loading process is illustrated in Figure 9. It can be seen that the dissipation of kinetic energy of the projectile was completely transformed into the internal energy of the structure, which could then be divided into three components: internal energy of the core, the front face-sheet and the back face-sheet.

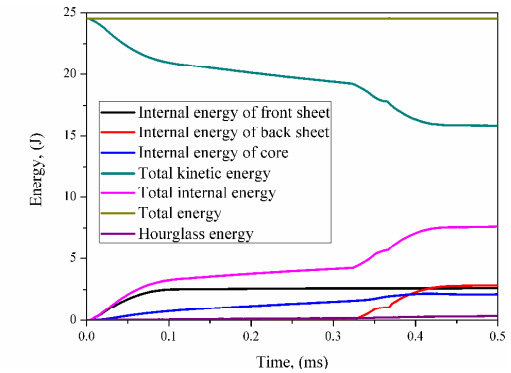

Figure 9: Energy history of the entire system.

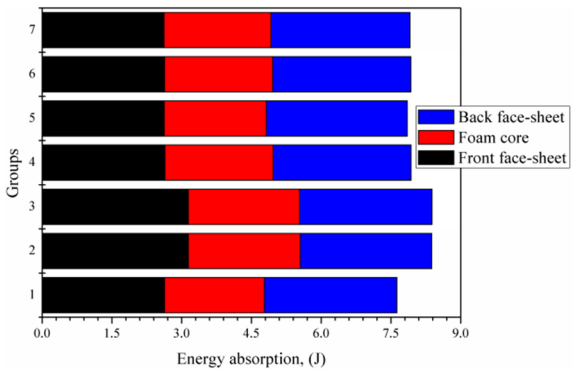

Figure 10: Comparison of the energy absorption of the components between the seven groups.

Figure 9 also indicates that the hourglass energy is very small in comparison with the total energy, and the total energy of the system is conservative during the penetration process. The above two points further guarantee the accuracy of the simulations.

The comparison of the energy absorption for each component of the sandwich shells with graded foam core is made in Figure 10. The comparison between Group 1 and the other groups demonstrate that the energy absorption of the uniform core is slightly smaller than the value of the graded cores. It indicates that the graded cores have a slightly positive influence on the energy absorption capacity of the sandwich structures. There are two reasons for this phenomenon. Firstly, in the case of those sandwich structures subjected to the impact loading, the energy absorption of the face-sheets accounted for over 70% of the total energy absorption, as shown in Figure 9 and Figure 10. In other words, the foam core is not the main component for energy absorption. Secondly, the diameter of the projectile is very small in comparison with the size of the sandwich structures, which directly leads to the structures' local damage. Therefore, the effect of the graded foam core on the energy absorption capacity of sandwich structures is not evident.

4.3 Impact phase diagram under the oblique impact

It is well known that the impact behavior of sandwich structures is influenced by various factors, such as the impact velocity and angle, the nose shape and diameter of the projectile, the dimensions and property of the target, etc. Details of these factors are presented in the following sections.

Figure 11 shows the oblique impact process of the sandwich shells under the impact of different projectiles. Three different terminal states of the projectiles - embedment, perforation and ricochet - are indicated. The effects of the terminal states of these projectile are an important topic in ballistic mechanics; therefore, the impact phase diagram is introduced to further analyze the oblique impact behavior.

A typical impact phase diagram is plotted in Figure 12. The ordinate and abscissa of the phase diagram represent the critical velocity and oblique angle, respectively. Each point in the impact phase diagram indicates the critical transition velocity, in which the transition state switches from one type to another. The terminal states of the projectile under different impact velocities can be observed, as shown in Figure 11. Therefore, the critical velocity can be acquired by observing the critical transition state of projectiles under different impact velocities. In brief, each point of transition in the impact

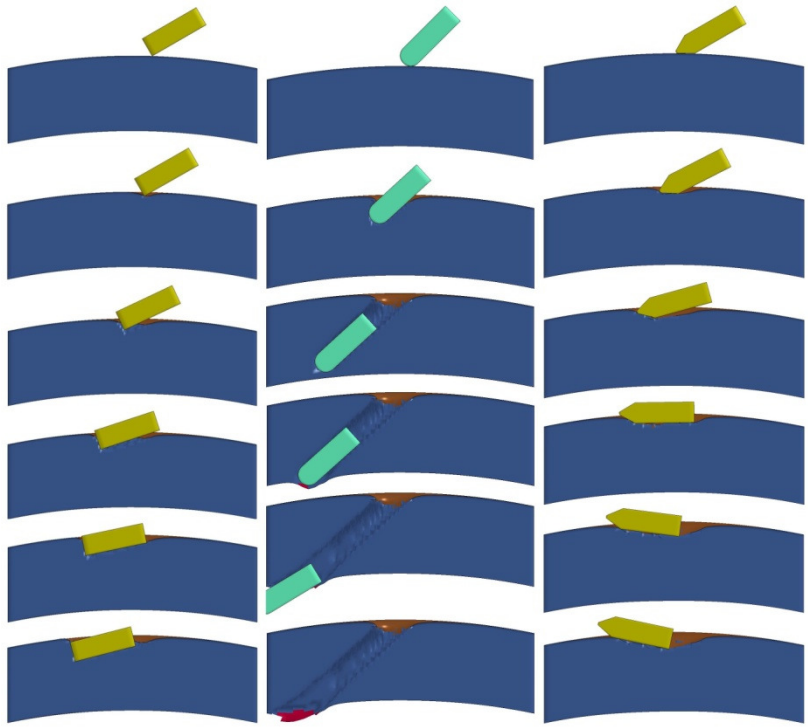

Figure 11: Oblique impact process of the sandwich shells with different projectiles impact. (a) embedment; (b) perforation; (c) ricochet.

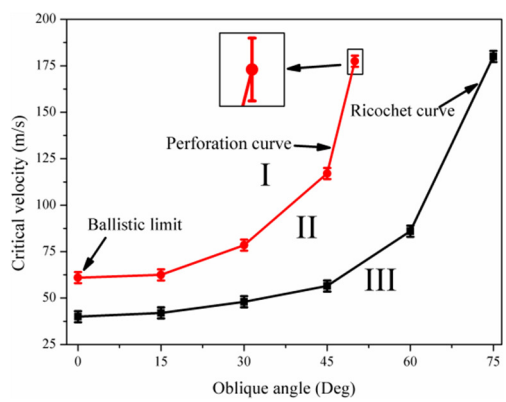

Figure 12: Schematic of impact phase diagram.

phase diagram is obtained by running many cases. However, it should be noted that the critical velocity is difficult to predict accurately, due to the critical transition state being very hard to distinguish (Zheng et al., 2005). Consequently, all of the critical velocities are estimated and have an error margin of ± 3 m/s.

Based on the results of critical velocity curves, the impact phase diagram of sandwich shell is divided into three region. The red curve is called a 'perforation curve' and reflects the critical velocity where the projectile perforates during the impact. Particularly, $\theta = 0°$ is the point on the perforation

curve that represents the ballistic limit. Similarly, the black curve is called a 'ricochet curve', which reflects the critical velocity in which the projectile ricochets. Regions I, II and III represent the perforation, embedment and ricochet states of the projectile, respectively. The impact phase diagram clearly indicates the influence of the impact velocity and the oblique angle on the terminal states of the projectile. In other words, it can properly predict the effects of key parameters on the impact-resistance performance of the target.

It can be seen from Figure 12 that both critical velocity curves vary stably at the initial stage, then rapidly increase with the increase of the oblique angle. This is because a larger oblique angle means the component of the normal direction of the target will decrease and a higher impact velocity is imperative. In addition, Figure 12 clearly shows that the scale of Region II increases with the rise of the oblique angle. It reveals that the larger oblique angle easily causes the embedment of the projectile. Further simulations can be found where the critical velocity is approximately infinity after a certain oblique angle, demonstrating that the projectile will not cause perforation or embedment under a certain oblique angle, regardless of how the impact velocity changes. Meanwhile, it should be noted that the critical perforation angle is smaller than the ricochet angle because of geometric dimension of the sandwich structure, and detailed analyses are discussed in Section 4.3.2.

4.3.1 Effect of projectile shape on the impact phase diagram

In order to analyze the effect of projectile nose shape, the diameter of projectile, the curvature and the thickness of the face-sheet were set as 8 mm, 4/m and 1 mm, respectively. The results of the projectile with three nose shapes were compared in Figure 13. For these curve results, the following observations can be made. Firstly, the ballistic limit of the flat nosed projectile is remarkably higher than the other projectiles. This conclusion has been obtained in Section 4.1.1. Secondly, the critical velocity curves of the hemispherical and conical projectile began to rise slowly and then rapidly increase with the increase of the oblique angle. Yet, for the flat projectile, there was a visible decline during the initial stage. It is because the small oblique angle ($\theta < 30°$) leads to the rapid decrease in the contact area between the flat projectile and the sandwich structure. Moreover, a smaller contact area results in higher contact stress and lower critical velocity. Thirdly, the critical velocity deviation between different projectile shapes gradually decreases with the oblique angle increasing, which indicates that the influence of the projectile shape in terms of normal penetration is greater than that of the oblique penetration.

4.3.2 Effect of face-sheet curvature on the impact phase diagram

In this section, the numerical models are used by a hemispherical nose projectile with diameter of 8 mm and the sandwich shell structures with face-sheet thickness of 1 mm. The values of the face-sheet curvature varied from 0/m to 8/m. Figure 14 is where the numerical results for the impact phase diagram with different face-sheet curvatures were plotted. It is clear that there is almost no difference in the ricochet curves until the oblique angle reaches nearly 50°. This phenomenon reveals that the curvature of the sandwich shells has little influence on the ricochet curves since the deformation is localized in a small area of the front face-sheet when the ricochet occurs, as shown in Figure 11 and Figure 15. Meanwhile, the variation caused by the curvature of the sandwich structure can be ignored

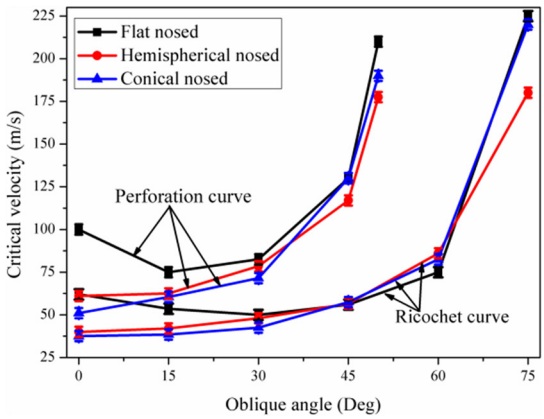

Figure 13: The impact phase diagram with different projectile shapes.

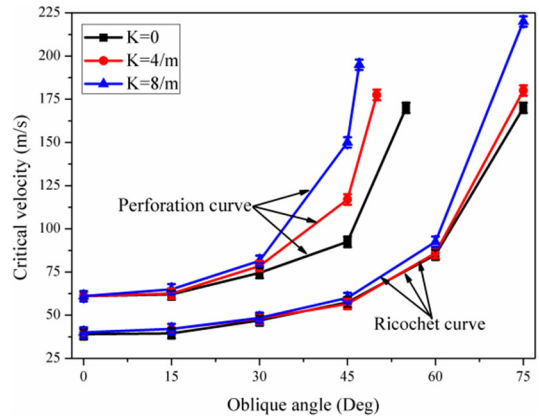

Figure 14: The impact phase diagram with different face-sheet curvatures.

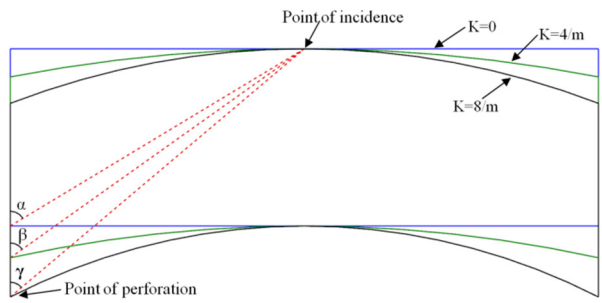

Figure 15: Schematic of the critical ricochet/perforation angle.

in this small area. Similarly, the face-sheet curvature has slight effects on the perforation curves when oblique angle θ is smaller than 30°. The primary reason for this phenomenon is similar to what is mentioned above. However, the influences of curvature become considerable with the value of the oblique angle further increasing. It is mainly contributed by the variation of the critical perforation angle. Figure 15 concisely shows the relationship between the face-sheet curvature and the critical perforation angle (i.e. α, β and γ). It is very clear that the critical perforation angle decreases with the increase of the face-sheet curvature.

The foregoing analysis suggests that the ricochet curve is controlled mainly by the front face-sheet of the sandwich structure and the ricochet angle is unrestricted, so it can be changed from 0 to 90°. On the other hand, the variation in the perforation curve is primarily determined by the critical perforation angle. Also, the critical perforation angle is restricted by many such factors as: face-sheet curvature, foam core thickness and sandwich structure dimension. Therefore, it has an upper limit. This is why the critical perforation angle is always smaller than the ricochet angle.

The penetration testing for sandwich structures with foam core have been carried out. Figure 16 shows the numerical and experimental deformation pattern of the back face-sheet for the sandwich panel ($K = 0$) under normal impact by the hemispherical nosed projectiles. It is found that the numerical results agree well with experimental failure modes and the experimental detailed results will be presented in other papers.

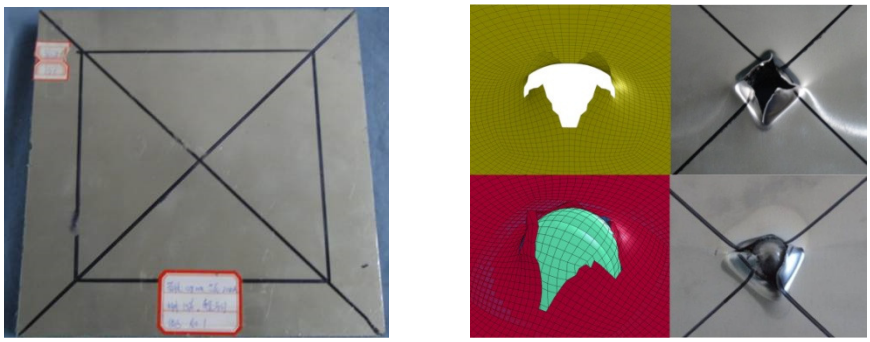

(a) (b)

Figure 16: Illustration of the specimen. (a) The undeformed schematic of the specimen; (b) Comparison of numerical and experimental deformation pattern under normal impact.

4.3.3 Effect of projectile diameter on the impact phase diagram

In this section, the numerical models are used by a hemispherical nose projectile and the sandwich shell structures with face-sheet thickness of 1 mm and curvature of 4/m, respectively. The simulation results are plotted in Figure 17. It is clear that the trend of variation for the three sets of phase diagram is basically consistent. Furthermore, using the results of the projectile with 8 mm diameter as a benchmark, the ballistic limit for projectiles with 9 mm and 10 mm diameter increase by 13.2% and 31.2%, respectively. It can be understood that projectile with larger diameter can efficiently increase the region of interaction and cause more face-sheets and foam cores to participate in the process of penetration. Therefore, the ballistic limit and impact-resistance performance of target can rise by increasing the diameter size of projectiles with the same mass.

4.3.4 Effect of face-sheet thickness on the impact phase diagram

In this section, the simulation used an 8 mm diameter projectile with hemispherical nose and the fixed the face-sheet curvature at 4/m. The influence of the face-sheet thickness on the impact phase diagram is shown in Figure 18. Obviously, the impact-resistance performance of the target enhance due to increasing the face-sheet thickness. Additionally, the effects of the thickness of face-sheet on the critical velocity are nonlinear. The deviation between the curves is nonlinear with the penetration angle. For instance, the difference of the ricochet critical velocity between $H = 0.8$ mm and $H = 1.2$ mm is 12 m/s (when $\theta = 15°$), but the difference turns to 35 m/s with the oblique angle increasing (when $\theta = 75°$). The same variation trend of the critical velocity with different geometric parameters can be observed in Figure 14 and Figure 17. It indicates that the critical velocity curves are sensitive to the geometric parameter in the case of a larger oblique angle.

In order to verify this particular phenomen, oblique angles are investigated in detail. The deflection angle curves of the projectile under the constant impact velocity are plotted against the impact time, as shown in Figure 19 for two different oblique angles. Here, the deflection angle is defined as the acute angle between the instantaneous and the initial axial direction of the projectile during oblique impact (Chen et al., 2005). It is clearly that the deflection angles are almost constant and are hardly influenced by sheet thickness for the $\theta = 15°$. For the $\theta = 75°$, however, the deflection angle curves rapidly increase during the penetration process and the deflection angles remarkably enlarge with

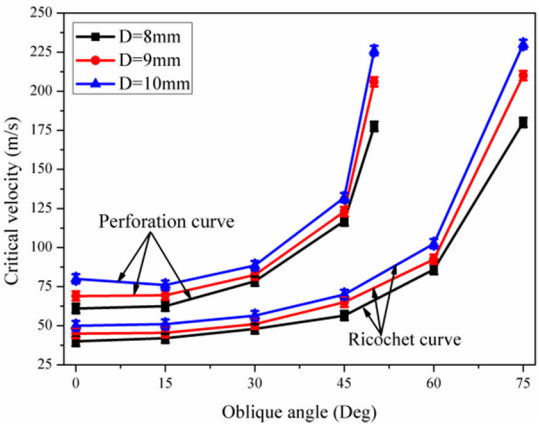

Figure 17: The impact phase diagram with different projectile diameters.

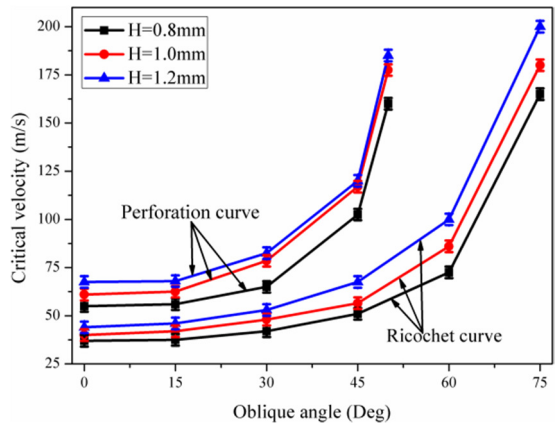

Figure 18: The impact phase diagram with different face-sheet thicknesses.

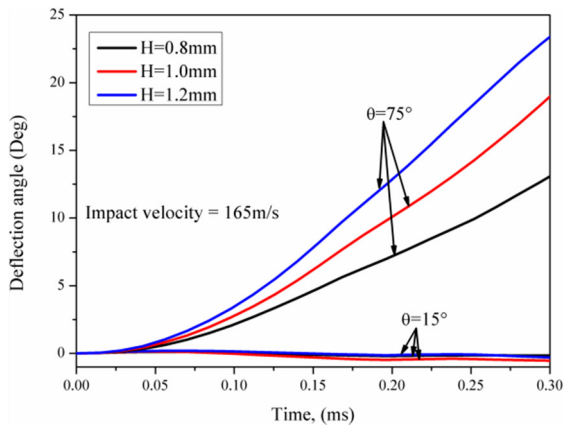

Figure 19: Plot of deflection angle curves versus time under two different oblique angles.

increasing sheet thickness. Figure 19 indicates that the deflection of projectile become easier and more susceptible to the material and geometric parameters of the entire system with the increase of the oblique angle. Obviously, a lager deflection angle, to a great extent, influences the terminal state of the projectile. In order to decrease the deflection of the projectile, the impact velocity has to be boosted significantly. Therefore, based on the above discussion of the impact phase diagrams it can be concluded that larger oblique angle can obviously increase the difference between the critical velocity curves.

5 CONCLUSIONS

Normal and oblique impact simulations were performed to predict the ballistic performance and the impact behavior of sandwich shell structures with both uniform and graded foam cores. The sandwich shells were subjected to impact by three kinds of projectiles: flat, hemispherical and conical nosed. The failure modes of the back face-sheet - i.e. plugging, petaling and hole enlargement - are sensitive to the projectile shapes. The results indicate that blunter projectile and higher impact velocity can significantly raise the energy absorption of the sandwich structures because of the larger deformation

area and the inertia effect of the structure, respectively. Furthermore, the graded foam cores do not exhibit evident effects on resisting the projectile impact and energy absorption due to the interaction region remaining relatively localised.

Based on the impact phase diagram obtained, the effects of several parameters - i.e. projectile shape and diameter, face-sheet curvature and thickness - on the normal/oblique impact behavior were analyzed. The impact phase diagram clearly indicates that the influence of the projectile shape on the normal penetration is greater than that on the oblique penetration. Larger diameter projectile and thicker sheets can effectively raise the ballistic limit and the impact-resistance performance of targets. Meanwhile, the critical perforation angle increases with the decrease of sheet curvature, finally resulting in the deviation of the perforation curve. In addition, larger oblique angles are prone to producing larger deflection of the projectile, further resulting in a greater difference of velocity curves.

Acknowledgements

This work is supported by the National Natural Science Foundation of China (Grant Nos. 11172195 and 11172196), the Top Young Academic Leaders of Shanxi and the Outstanding Innovative Teams of Higher Learning Institutions of Shanxi. The financial contributions are gratefully acknowledged.

References

Ashby, M.F., Evans, A.G., Fleck, N.A., Gibson, L.J., Hutchinson, J.W., Wadley, H.N.G., (2000). Metal foams: a design guide. Oxford: Butterworth-Heinemann.

Buitrago, B.L., Santiuste, C., Sánchez-Sáez, S., Barbero, E., Navarro, C., (2010). Modelling of composite sandwich structures with honeycomb core subjected to high-velocity impact. Composite Structures 92: 2090-96.

Chen, X.W., Fan, S.C., Li, Q.M., (2005). Oblique and normal perforation of concrete targets by a rigid projectile. International Journal of Impact Engineering 30: 617–637.

Cho, J.U., Hong, S.J., Lee, S.K., Cho, C.D., (2012). Impact fracture behavior at the material of aluminum foam. Materials Science and Engineering A 539: 250-58.

Dean, J., S-Fallah, A., Brown, P.M., Louca, L.A., Clyne, T.W., (2011). Energy absorption during projectile perforation of lightweight sandwich panels with metallic fibre cores. Composite Structures 93: 1089-95.

Deshpande, V.S., Fleck, N.A., (2000). Isotropic constitutive models for metallic foams. Journal of the Mechanics and Physics of Solids 48: 1253-83.

Fleck, N.A., Deshpande, V.S., (2004). The resistance of clamped sandwich beams to shock loading. Journal of Applied Mechanics 71: 1–16.

Gibson, L.J., Ashby, M.F., (1997). Cellular solids: structure and properties. 2nd ed. Cambridge: Cambridge University Press.

Gupta, N.K., Iqbal, M.A., Sekhon, G.S., (2008). Effect of projectile nose shape, impact velocity and target thickness on the deformation behavior of layered plates. International Journal of Impact Engineering 35: 37-60.

Hanssen, A.G., Girard, Y., Olovsson, L., Berstad, T., Langseth, M., (2006). A numerical model for bird strike of aluminium foam-based sandwich panels. International Journal of Impact Engineering 32: 1127-44.

Hou, W.H., Zhu, F., Lu, G., Fang, D.N., (2010). Ballistic impact experiments of metallic sandwich panels with aluminium foam core. International Journal of Impact Engineering 37: 1045-55.

Iqbal, M.A., Gupta, G., Gupta, N.K., (2010). 3D numerical simulations of ductile targets subjected to oblique impact by sharp nosed projectiles. International Journal of Solids and Structures 47: 224-37.

Ivañez, I., Santiuste, C., Barbero, E., Sanchez-Saez, S., (2011). Numerical modelling of foam-cored sandwich plates under high-velocity impact. Composite Structures 93: 2392-99.

Jing, L., Wang, Z.H., Ning, J.G., Zhao, L.M., (2011). The dynamic response of sandwich beams with open-cell metal foam cores. Composites: Part B 42: 1–10.

Jing, L., Xi, C.Q., Wang, Z.H., Zhao, L.M., (2013). Energy absorption and failure mechanism of metallic cylindrical sandwich shells under impact loading. Materials and Design 52: 470-80.

Keyword user's manual, (2012). Livermore Software Technology Corporation.

Li, S.Q., Wang, Z.H., Wu, G.Y., Zhao, L.M., Li, X., (2014). Dynamic response of sandwich spherical shell with graded metallic foam cores subjected to blast loading. Composites: Part A 56: 262-71.

Lu, G., Shen, J., Hou, W., Ruan, D., Ong, L.S., (2008). Dynamic indentation and penetration of aluminium foams. International Journal of Mechanical Sciences 50: 932-43.

Lu, G., Yu, T.X., (2003). Energy absorption of structures and materials. Cambridge: Woodhead Publishing Ltd.

Mohan, K., Yip, T.H., Idapalapati, S., Chen, Z., (2011). Impact response of aluminum foam core sandwich structures. Materials Science and Engineering A 529: 94-101.

Mozafari, H., Khatami, S., Molatefi, H., (2015). Out of plane crushing and local stiffness determination of proposed foam filled sandwich panel for Korean Tilting Train eXpress – Numerical study. Materials and Design 66: 400–411.

Qiu, X., Fleck, N.A., (2003). Finite element analysis of the dynamic response of clamped sandwich beams subject to shock loading. European Journal of Mechanics - A/Solids 22: 801-14.

Senthil, K., Iqbal, M.A., (2013). Effect of projectile diameter on ballistic resistance and failure mechanism of single and layered aluminum plates. Theoretical and Applied Fracture Mechanics 67: 53-64.

Shen, J.H., Lu, G., Ruan, D., (2010a). Compressive behaviour of closed-cell aluminium foams at high strain rates. Composites: Part B 10: 678–685.

Shen, J.H., Lu, G., Wang, Z.H., Zhao, L.M., (2010b). Experiments on curved sandwich panels under blast loading. International Journal of Impact Engineering 37: 960-970.

Shen, J.H., Lu, G., Ruan, D., Chong, C.S., (2015). Lateral plastic collapse of sandwich tubes with metal foam core. International Journal of Mechanical Sciences 91: 99–109.

Tan, P.J., Reid, S.R., Harrigan, J.J., Zou, Z., Li, S., (2005). Dynamic compressive strength properties of aluminum foams Part II-'shock' theory and comparison with experimental data and numerical models. Journal of the Mechanics and Physics of Solids 53: 2206–30.

Zhao, H., Elnasri, I., Girard, Y., (2007). Perforation of aluminium foam core sandwich panels under impact loading-An experimental study. International Journal of Impact Engineering 34: 1246-57.

Zheng, Z.J., Yu, J.L., Li, J.R., (2005). Dynamic crushing of 2D cellular structures: A finite element study. International Journal of Impact Engineering 32: 650–664.

Zhou, Z.W., Wang, Z.H., Zhao, L.M., Shu, X.F., (2012a). Experimental investigation on the yield behavior of Nomex honeycombs under combined shear-compression. Latin American Journal of Solids and Structures 9: 515-30.

Zhou, Z.W., Wang, Z.H., Zhao, L.M., Shu, X.F., (2012b). Loading rate effect on yield surface of aluminum alloy foams. Materials Science and Engineering A 543: 193-99.